Chapter 5

Cu_2ZnSnS_4 Thin Film Solar Cells: Present Status and Future Prospects

Minlin Jiang and Xingzhong Yan

Additional information is available at the end of the chapter

http://dx.doi.org/10.5772/50702

1. Introduction

Pollution of the earth and shortage of energy sources have been the bottle-neck of survival and development for human beings since the start of the 21st century. Therefore, lowering energy consumption and protecting the environment have gradually gained attention from countries all over the world. In order to keep sustainable development, governments, research institutes, and industries have been working on the problems caused by the shortage of available energy sources. It is well known that the best way is to exploit renewable energy resources. Solar energy is considered to be the most economic and effective among all available renewable energy resources. Solar energy is inexhaustible and it has already been theoretically and experimentally proved that the earth would not be polluted at all if solar energy was utilized effectively.

To encourage and to promote the direct utilization of solar energy, developed countries have been legislating and deploying solar initiatives [1-3]. Joint Research Centre (Europe) predicted that energy directly harvested from sunlight would be 20% of total energy consumption in 2050, and this value could be over 50% in 2100 [4]. Solar energy will be widely utilized in industry, agriculture and daily life. Photovoltaic (PV) systems have recently attracted much attention due to their inherent advantages. Firstly, PV systems are capable of directly translating sunlight into electrical energy. The theoretical conversion efficiency of PV systems is relatively higher than other power generators. Secondly, PV systems do not necessarily contain movable parts. System wear induced by mechanical movement is avoided. Therefore, PV systems can work continuously free from maintenance longer than other power generation technologies.

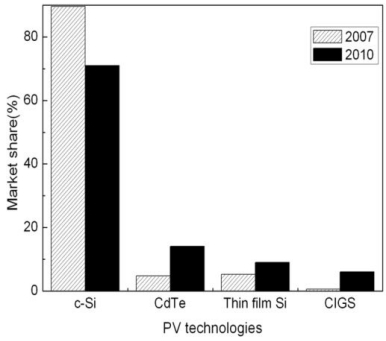

Figure 1. Market share of different PV technology [8].

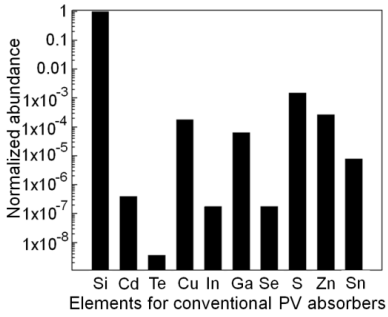

Figure 2. Normalized abundance of elements for conventional PV absorbers.

It was reported by Solarbuzz that 16.3 GW PV modules had been shipped to customers in 2010 with the lion's share going to crystalline silicon (c-Si) technology (71%) [5]. Due to high cost and energy consumption input in manufacturing c-Si PV of modules, market share of the c-Si technology has been dropping while thin film PV technologies have been increasing rapidly [6, 7]. There are three main thin film PV technologies, CdTe, $CuInxGa_{1-x}S(Se)_2$ (CIGS), and thin film Si, which has gained 14%, 9%, and 6% of PV market share in 2010, respectively (Fig.1) [8]. Nevertheless, Si thin film solar cell (TFSC) has been relatively underdeveloped due to low efficiency and instability from the Staebler–Wronski effect. For the other two thin film technologies, there are restriction on the usage of heavy metals such as cadmium, the limitation in supplies for indium and tellurium, and the wide fluctuation in prices of indium and tellurium. These render the combined production capacity of the existing CdTe and CIGS technologies at a small scale lower than 100 GW per year. This is only a small fraction of energy consumption in 2050 which is expected to be 27 TW [4, 9].

Recently, quaternary compound Cu_2ZnSnS_4 (CZTS) has been intensively examined as an alternative PV material due to its similarity in material properties with CIGS and the relative abundance of raw materials (Fig. 2). CZTS is a compound semiconductor of $(I)_2(II)(IV)(VI)_4$.

http://dx.doi.org/10.5772/50702

With a high absorption coefficient (> 10^4 cm^{-1}) and a desirable bandgap (~1.45 eV), CZTS thin film has been considered an excellent PV material. Theoretical calculations have shown that conversion efficiency as high as 32% was possible for CZTS TFSCs with a CZTS layer of several micrometers. Wadia et al. also calculated the minimum cost of raw materials for the existing PV technologies and the emerging PV technologies [10]. Part of the results is shown in Fig. 3. The cost of raw material for CZTS PV technology is much lower than that of the three existing thin film PV technologies.

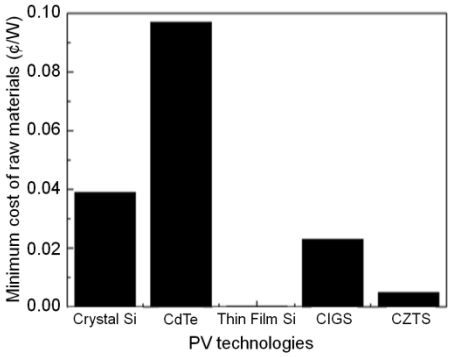

Figure 3. Minimum cost of raw materials for different PV technology [10].

Significant progress on this relatively new research area has been achieved in last five years. Champion efficiency of CZTS thin film solar cell (TFSC) has reached 8.4 % and an efficiency of 6.21 % has been demonstrated for CZTS sub-module with an area of 22.6 cm^2. However, these efficiencies are still much lower than those of CIGS PV devices. This chapter reviews the present status of various CZTS TFSC technologies with special emphasis on properties of CZTS thin films deposited by different methods. New results generated by solution-based processing have been reported, and the methodologies to make CZTS photovoltaic technology more marketable are also proposed and discussed. Based on the information reported and our experiences gained on the research and development of CIGS and CZTS solar cells, the challenges and perspectives of CZTS TFSCs have been addressed.

2. General properties of CZTS thin film

In 1967, CZTS single crystal was synthesized and analyzed [11]. However, it had not gained intensive interest from academies and industries until 2007 when solar power was heavily subsidized by governments and Si-based PV technologies encountered a skyrocketing price of highly pure polycrystalline silicon. Thus far, structural, optical, and electrical properties of CZTS thin film have been intensively investigated.

2.1. Crystal structure

CZTS thin films are usually in a polycrystalline form consisting of kesterite crystal structures. Kesterite CZTS single crystal was first synthesized by Nitsche et al. using the chemical vapor transport method [11]. X-ray diffraction (XRD) results showed that this synthesized CZTS had sphalerite-like crystal structure with c/a being close to 2 (a=5.43 Å, c=10.83 Å). In 1974, detailed lattice data of a CZTS single crystal were reported by Schäfer and Nitsche (Table 1) [12]. Thereafter, this data was frequently referenced to determine CZTS phase in literatures. In 2011, Lu et al. claimed that wurtzite CZTS nanocrystals were synthesized through a hot injection method [13]. The experimental XRD patterns were indexed to a simulated crystal structure with a wurtzite phase (Table 2).

d (Å)	I/I_0 (%)	(hkl)	2θ (degree)
5.421	1	002	16.338
4.869	6	101	18.205
3.847	2	110	23.101
3.126	100	112	28.530
3.008	2	103	29.675
2.713	9	200	32.989
2.426	1	202	37.025
2.368	3	211	37.966
2.212	1	114	40.758
2.013	2	105	44.996
1.919	90	220	47.331
1.636	25	312	56.177
1.618	3	303	56.858
1.565	10	224	58.969
1.45	1	314	64.177
1.356	2	008	69.229
1.245	10	332	76.442

Table 1. Lattice data of the kesterite CZTS single crystal [12].

Notes: d indicates the distance between two neighbor parallel planes, I/I_0 is the relative peak intensity, (hkl) are Miller indexes, and 2θ is the twice of Bragg diffraction angle.

Kesterite CZTS has highly similar crystal structure with chalcopyrite CIGS where half of indium and (or) gallium is replaced by zinc and the other half by tin (Fig. 4(a)). Similar to ZnO or ZnS, the anions and cations in kesterite CZTS crystal are located in a tetrahedral bonding envi-

http://dx.doi.org/10.5772/50702

ronment with a stacking model which is similar to zincblende (Fig. 4(c)) [14]. The other important structure for CZTS crystal is a stannite structure (Fig. 4(d)) [14]. The difference between kesterite CZTS crystal and stannite CZTS crystal lies in a different order in the cation sub-lattice. In kesterite CZTS, cation layers of CuSn, CuZn, CuSn, and CuZn alternate at z = 0, 1/2, 1/2, and 3/4, respectively; while in stannite structures, ZnSn layers alternate with Cu_2 layers. The wurtzite structure can be formed by replacing Zn (II) with Cu (I), Zn (II) and Sn (IV) in wurtzite ZnS with each sulfur atom equally coordinating with two Cu (I), one Zn (II), and one Sn (IV) (Fig. 4(b)) [13]. First-principle calculations by Chen et al. indicated that the kesterite structure had a lower energy and should be more stable than the stannite structure [15]. Most of CZTS samples crystallized in the kesterite structure as predicted theoretically. XRD results showed that diffraction peaks of (112), (200), (220/204), and (312/116) with a preferred orientation along (112) were commonly observed [16-19]. Peaks of (002), (008), (101), (103), (105), (110), (211), (213), (224), and (332) were also demonstrated in the XRD spectra [20- 24].

Experimental *d* (Å)	Calculated *d* (Å)	(*hkl*)	Experimental 2*θ* (degree)
3.339	3.324	100	26.70
3.175	3.169	002	28.10
2.954	2.944	101	30.26
2.299	2.294	102	39.19
1.921	1.919	110	47.32
1.783	1.783	103	51.23

Table 2. Lattice data of the wurtzite CZTS crystal [13].

2.2. Optical properties

The optical bandgap of stoichiometric kesterite-CZTS was theoretically determined to be 1.50 eV [15]. Experimental results demonstrated that bandgap of CZTS thin film deposited using different method varied from 1.4 eV to 1.5 eV [16, 19, 20, 25, 26]. It is commonly recognized that CZTS thin film has an absorption coefficient as high as 10^4 cm^{-1}. Sol-gel derived CZTS thin film from our group confirmed that the absorption coefficient is higher than 10^4 cm^{-1} in the photon energy range greater than 1.2 eV (Fig. 5) [27].

Raman spectrum is a powerful characterization method to reveal Raman shift peaks in CZTS especially for the peaks associated with secondary phases such as Cu_xS, ZnS, Sn_xS, Cu_2SnS_3, and Cu_3SnS_4. The universally acknowledged peak is 338 cm^{-1} [28]. However, peaks at 96 cm^{-1}, 166 cm^{-1}, 250 cm^{-1}, 251 cm^{-1}, 287 cm^{-1}, 288 cm^{-1}, 289 cm^{-1}, 337 cm^{-1}, 338 cm^{-1}, 352 cm^{-1}, 370 cm^{-1}, 372 cm^{-1} have also been observed and assigned to CZTS [16, 29-32].

To study the recombination mechanisms, low temperature photoluminescence spectra were recorded from CZTS thin films. Several groups observed a broad peak centering at around 1.24 eV, which was attributed to the typical donor-acceptor pair transition involving tail states created by potentials fluctuations [33-35]. It is claimed that the presence of potential

fluctuations indicates CZTS is strongly compensated [33]. Time-resolved PL data illustrated that lifetime of free carriers in CZTS thin film was lower than 1 ns [36].

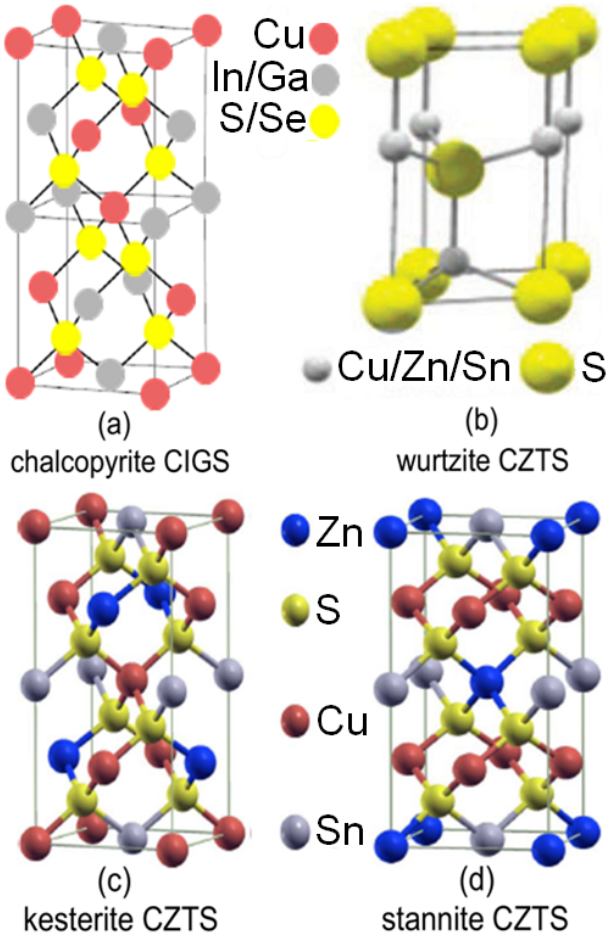

Figure 4. Crystal structures of CIGS and CZTS [13, 14].

2.3. Electrical properties

In contrast with silicon, where either atoms of phosphorus or atoms of boron are intentionally introduced for producing n-type and p-type semiconductors, respectively, CZTS is self-doped through a formation of intrinsic defects including vacancies (V_{Cu}, V_{Zn}, V_{Sn}, and V_S), antisite defects (Cu_{Zn}, Zn_{Cu}, Cu_{Sn}, Sn_{Cu}, Zn_{Sn}, and Sn_{Zn}), and interstitial defects (Cu_i, Zn_i, and Sn_i). These defects could form during growth of CZTS thin film. Chen et al. systematically studied the defect properties of CZTS using first-principle calculations [37]. It was found

http://dx.doi.org/10.5772/50702

that the formation energy of acceptor defects was lower than that of donor defects, which makes n-type doping very difficult in CZTS [37]. The commonly observed p-type conductivity of CZTS thin films comes mainly from the Cu_{Zn} antisite defect, partly explaining why CZTS thin films must be Cu-poor and Zinc-rich to successfully fabricate CZTS solar cells.

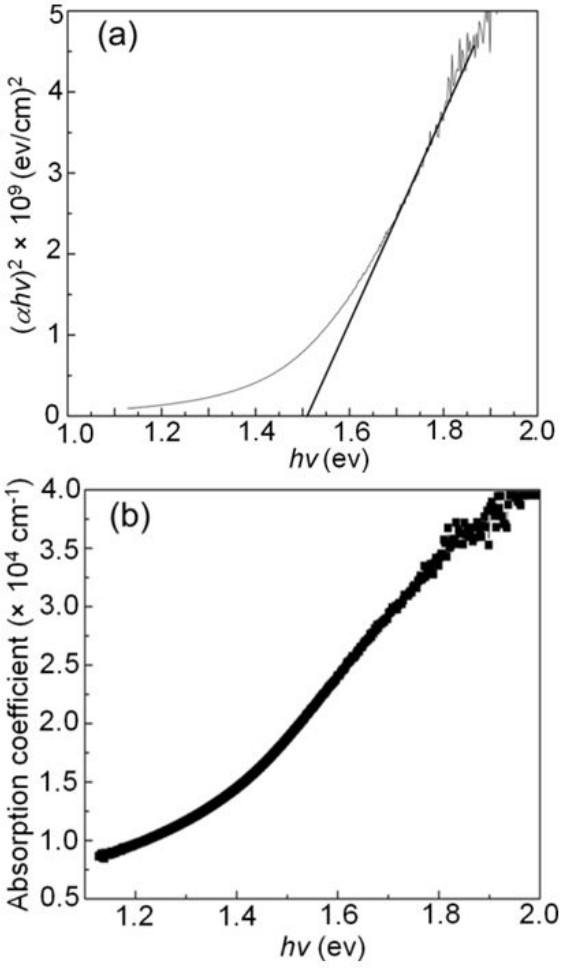

Figure 5. a) Typical bandgap and (b) absorption coefficients of a CZTS thin film [27].

Reported resistivity of CZTS thin films was significantly different [38-40]. The most suitable value for CZTS thin film should range from $10^{-3}\Omega\bullet$cm to $10^{-1}\Omega\bullet$cm according to published data for CZTS solar cells [25]. The hole concentration was reported to vary from 10^{16}cm^{-3} to 10^{18}cm^{-3} [41-43], although extremely high and extremely low concentration were also report-

ed [44, 45]. Hall effect measurement results showed that hole mobility of CZTS changed from lower than 0.1 to as high as 30 $cm^2 \bullet V^{-1} \bullet s^{-1}$, while most published values were in the range of 1 to 10 $cm^2 \bullet V^{-1} \bullet s^{-1}$ [40, 44-47]. The lower mobility indicates that the optimized thickness of absorber layer in CZTS TFSCs cannot be as large as that for CIGS TFSCs.

3. CZTS thin film solar cell

We would like to first introduce the basic definitions which are very important parameters when evaluating a solar cell. The solar cell can be basically taken as a battery in a simple electrical circuit (Fig. 6 (a)). Without sunlight shining on solar cell, it can do nothing. However, the solar cell will work as a battery if it is activated by light (Fig. 6 (b)). Electrical potential difference will be developed between its two ends and electrical current can flow through the solar cell. The potential difference derived when the resistance of the load is infinite is defined as open circuit voltage, V_{OC}. Correspondingly, the electrical current flowing in the circuit when the resistance of the load is zero is defined as short circuit current, J_{SC}. Shown in Fig. 6 (c) is a typical *I-V* relationship curve of the illuminated solar cell when the load resistance changes from zero to infinite. The delivered power by the solar cell, *P*, is given by

$$P = I \times V \tag{1}$$

The typical *P-V* relationship curve is also shown in Fig. 6 (c). *P* reaches a maximum value at certain condition under which the solar cell will deliver the highest power to the external load. This condition is defined as maximum power point and the maximum power is denoted as P_m. The corresponding voltage and current is denoted as V_m and I_m, respectively. Another important parameter to evaluate a solar cell is fill factor, *FF*, which is defined as

$$FF = \frac{I_{\mathrm{m}} \times V_{\mathrm{m}}}{I_{\mathrm{SC}} \times V_{\mathrm{OC}}} \tag{2}$$

The most important parameter for a solar cell is conversion efficiency, η, which describes the solar cell's ability to translate solar energy into electrical energy. The conversion efficiency is given by

$$\eta = \frac{P_{\mathrm{m}}}{P_{\mathrm{L}}} \tag{3}$$

where P_L is the power of the simulated light.

Parameters such as J_{SC}, V_{OC}, *FF*, and η are key performance characteristics of a solar cell. These parameters are light-dependent and environment-dependent, which means that the values of these parameters of a specific solar cell will change if the solar cell is illuminated with different light intensity. Worldwide recognized characterization condition for solar cells is the

http://dx.doi.org/10.5772/50702

Standard Test Condition (STC) which stipulates that a solar cell should be tested at 25℃ under Air Mass 1.5 spectrum illumination with an incident power density of 100 mW/cm^2.

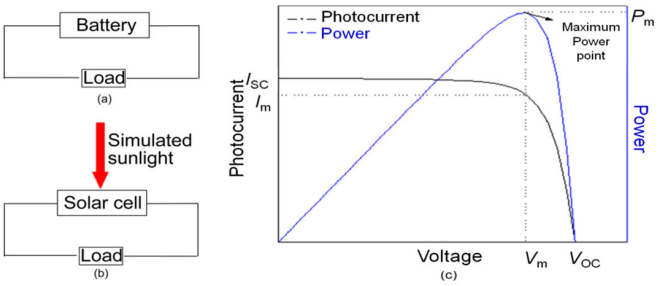

Figure 6. a) Schematic basic electrical circuit, (b) schematic basic operating circuit of solar cell, (c) typical I-V curve of a solar cell.

3.1. Basic structure and fabrication procedures

The schematic structure of CZTS solar cell is shown in Fig.7. Molybdenum thin film with thickness of 500~700 nm is sputtering-deposited on glass substrate as back contact because Mo is stable in harsh reactive conditions such as sulfur-containing vapor and high temperature. The absorber layer, p-type CZTS thin film with thickness ranging from 1.0 to 2.0 μm is then coated on Mo thin film. To form p-n junction with the p-type CZTS, 50~100 nm n-type CdS thin film is deposited on the absorber layer usually by chemical bath deposition. The surface of CZTS thin film is too rough to be fully covered by CdS thin film, leading to shortage between front contact and back contact. To prevent leakage, 50~90 nm intrinsic ZnO (i-ZnO) thin film is usually sputtering-coated on CdS before 500~1000 nm transparent conducting oxide (TCO) thin film is deposited by sputtering as the front contact layer of the cell. Finally, to electrically measure the *I-V* property of CZTS solar cell, Ni/Al grid is separately deposited on both TCO and Mo layer.

3.2. Deposition techniques of CZTS thin films

The first $(I)_2(II)(IV)(VI)_4$ solar cell was developed in 1977 by Wagner and Bridenbaugh. A n-type CdS thin film was evaporation-coated on vapor transportation-grown Cu_2CdSnS_4 single crystal substrate to form the p-n junction [48]. This device showed a short-circuit current density of 7.9 mA/cm^2, an open-circuit voltage of 0.5 V, and a conversion efficiency of 1.6%. The authors pointed out that a large series resistance limited the performance. In 1988, a heterojunction solar cell with an open circuit voltage of 165 mV was achieved by depositing cadmium tin oxide on CZTS thin film [40]. In 1997, the first CZTS TFSC with efficiency of 0.66% was realized by Katagiri using electron beam deposition followed by sulfurization [49]. The highest efficiency of 8.4% for CZTS TFSC and 6.21% for sub-module has been achieved by IBM and by Solar Frontier, respectively [36, 50].

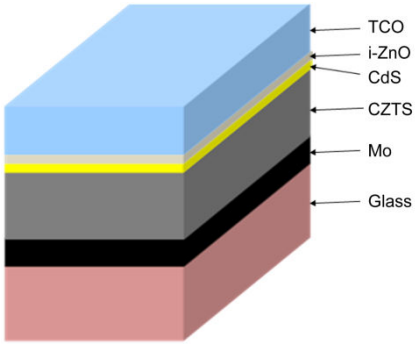

Figure 7. Schematic structure of typical CZTS solar cell.

Shown in Fig.8 are conversion efficiencies for CZTS solar cells obtained by different methods. Evaporation and sputtering have been intensively employed for the deposition of CZTS thin film both because the properties of CZTS thin film are more readily controlled using these two methods and because great success has been achieved experimentally and commercially for CIGS solar cells manufactured using evaporation and sputtering.

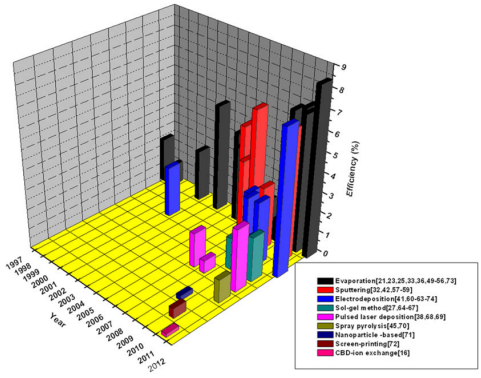

Figure 8. Conversion efficiencies obtained for CZTS solar cells by different methods.

The highest efficiencies achieved by the specific methods shown in Fig. 8 are listed in Table 3. Many technologies have been explored for fabricating CZTS TFSCs, as discussed in detail in the following paragraphs. Similar to the CIGS solar cells, whose highest efficiency was obtained by evaporation deposition [75], the highest efficiency of CZTS solar cell was also attained by evaporation deposition [36]. Conversion efficiency of 10.1% by IBM and 7.23% by Guo et al. have been realized for $Cu_2ZnSn(S,Se)_4$ (CZTSSe) solar cells made using solution-based method and nanoparticle-based method, respectively [76,77]. However, both cas-

http://dx.doi.org/10.5772/50702

es modified the composition of CZTS thin films through introduction of selenium, which is a rare element in the earth crust.

Method	Precursor	Efficiency (%)	Year	Reference
Evaporation	Cu, Zn, Sn, S	8.4	2011	[73]
Sputtering	Cu, SnS, ZnS	6.77	2008	[59]
Electrodeposition	Cu(II) ion, Zn(II) ion, Sn(IV) ion	7.3	2012	[74]
Sol gel-based method	Copper (II) acetate monohydrate zinc (II) acetate dehydrate tin (II) chloride dehydrate	2.23	2011	[66]
Pulsed laser deposition	in-house fabricated CZTS pellet	3.14	2011	[69]
Spray pyrolysis	not available	1.15	2011	[70]
NP-based method	Copper(II) acetylacetonate, zinc acetate, tin(II) chloride dehydrate, elemental sulfur	0.23	2009	[71]
Screen-printing	CZTS microparticle	0.49	2010	[72]
CBD-ion exchange	tin chloride dehydrate, zinc acetate dehydrate, aqueous Cu^{2+}	0.16	2011	[16]

Table 3. Highest efficiency achieved for CZTS solar cell by different method.

3.3.1. Evaporation

Evaporation is a well-known technique in the development of thin film solar cells. In 1997, Katagiri et al. reported electron beam evaporation-deposited CZTS precursor films followed by sulfurization [49]. Solar cell with an efficiency of 0.66% was obtained. In this work, Zn, Sn and Cu layers were sequentially deposited on Mo-coated soda lime glass substrates which were heated up to 150 ℃. The targeted composition ratio was decided by the thickness of metallic layers. Annealing at 500 ℃ in the atmosphere of N_2 + H_2S (5%) was then employed to transform Cu/Sn/Zn stacked layers into a CZTS thin film. Finally, chemical bath deposition was employed to deposit n-type CdS thin film on the p-type CZTS to form a p-n junction. As a result, the open-circuit voltage was significantly enhanced in comparison to the previously reported value [40].

Similar deposition procedures were performed by the same group in 2001 with a replacement of Zn metal source by ZnS [25]. Also, the annealing temperature was increased to 550 ℃. CZTS thin films with thickness of 0.95 μm, 1.34 μm, and 1.63 μm were deposited on Mo-coated SLG substrates, respectively. The *J-V* results demonstrated that the short-circuit current density and the fill factor of these cells drastically decreased with the increase of thickness of CZTS thin film (Table 4). The authors concluded that the extremely high series resistance of CZTS absorber layer was attributed to the significant degradation encountered in the CZTS solar cells. Similar dependence of performance on the thickness of CZTS ab-

sorber layer was demonstrated in 2010 by Wang et al. (Table 4) [56]. Capacitance-voltage measurement results showed that the density of uncompensated charge in the CZTS layer was to be 5×10^{16} cm^{-3} at 27 ℃, which indicates that part of the high series resistance comes from the bulk CZTS absorber layer. Evaluation of the dependence of R_s on temperature from dark *J-V* curve provides insight on another potential source for the series resistance (Fig. 9). The strong dependence indicates a back-contact blocking (Schottky) barrier exists at the interface between CZTS and Mo, leading to the suppression of holes transporting across the interface to Mo.

R & D group	Thickness (nm)	J_{SC} (mA/cm^2)	V_{OC} (mV)	*FF* (%)	η (%)
Katagiri et al.	950	7.01	415	50.3	1.46
	1340	3.41	425	26.5	0.384
	1630	1.53	525	26.6	0.214
Wang et al.	650	17.8	587	65	6.81
	660	20.4	620	52	6.63
	900	18.3	640	38	4.40
	1200	14.4	608	28	2.44

Table 4. Comparison of *I-V* properties of CZTS TFSCs with different thickness of absorber layer [25, 56].

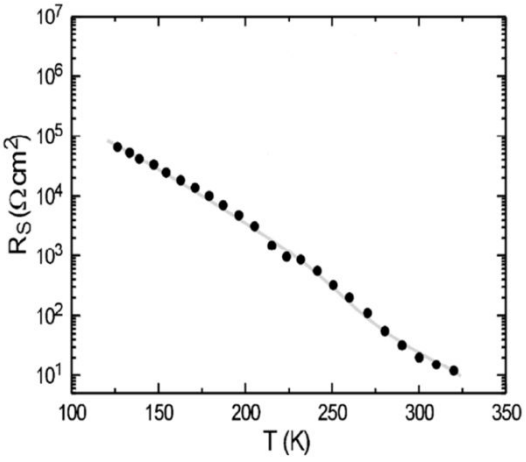

Figure 9. The dependence of R_s on temperature [56].

The large dependence of physical properties of CIGS thin film on the ratio of Cu/(In+Ga) suggests that it is necessary to investigate the effects of Cu/(Zn+Sn) ratio on the properties of CZTS films to further the understanding of CZTS solar cells [78]. In 2010, Tanaka et at. em-

http://dx.doi.org/10.5772/50702

ployed evaporation method to fabricate CZTS samples with constant Zn/Sn and S/metal ratios of 1.1 and 0.93 and with Cu/(Zn+Sn) ratio varying from 0.82 to 1.06 [79]. All samples were determined to be kesterite structure. XRD data showed that FWHM of the diffraction peak of (112) plane became narrower, and the $I_{(112)}/I_0$ increased with increasing Cu/(Zn+Sn) ratio. This indicated that the increasing of Cu/(Zn+Sn) ratio helped improve the crystallinity of CZTS films (Fig. 10 (a)). Surface SEM images of the CZTS films demonstrated that the grain size also increased with increasing Cu/(Zn+Sn) ratio (Fig. 10 (b)), suggesting deposition process containing Cu-rich condition could be developed for growing high-quality CZTS thin films. The champion CIGS solar cell was fabricated using three-stage co-evaporation method where CIGS thin film was changed to Cu-rich in the second stage from Cu-poor in the first stage. In the last stage, the Cu source was blocked and Ga, In, and Se were simultaneously deposited to restore the Cu-poor state. Similar procedures have yet to be proved effective for CZTS solar cells.

Na incorporation into the CIGS polycrystalline thin film is a necessary process to fabricate CIGS modules with high efficiency. The enhancement of efficiency largely comes from higher open-circuit voltage, improvement of fill factor, increasing of p-type conductivity as well as improvement of crystallinity of (112)-oriented CIGS films [80-82]. Na incorporation was performed for evaporated-CZTS solar cell by Katagiri et al. using Na_2S as Na source [54]. It was found that the efficiency was enhanced from 4.25% to 5.45%. This enhancement is mainly due to the increase of short-circuit current density which increased significantly from 10.3 mA/cm^2 to 15.5 mA/cm^2. The open-circuit voltage and fill factor were slightly lower than the CZTS solar cells without Na incorporation. While why the efficiency was improved was not mentioned in the paper, it can be assumed that Na incorporation can improve the quality of CZTS thin film at different mechanism compared with CIGS thin film. The effects of Na incorporation for improving the quality of CZTS thin film has been addressed by Jampana et al. [83]. CZTS thin films were deposited on soda-lime glass (SLG) and low-alkaline glass (LAG). An increase in grain size and an improvement of morphology were obviously demonstrated in CZTS thin films deposited on SLG (Fig. 11 (a) and Fig. 11 (b)). However, our experiment results indicated that no significant difference could be detected from CZTS thin films deposited on SLG and low-alkaline glass (Fig. 11 (c) and Fig. 11 (d)). The wide variation among effects of sodium incorporation on CZTS thin films possibly partly arises from the difference of deposition methods. The other explanation could be tracked to the lack of precision by only changing substrate type. More experiments have to be carried out on sodium-free substrate by exactly controlling the doping amount of sodium before sodium incorporation can be effectively employed to improve the performance of CZTS PV devices.

In 2011, IBM reported a champion efficiency of 8.4% was achieved for CZTS solar cell which was grown on Mo-coated SLG substrates by thermal evaporation using elemental Cu, Zn, Sn, and S as sources [36]. A cracker, which can increase the reactivity of S, was applied to S vapor. The employment of cracker probably helped improve the efficiency.

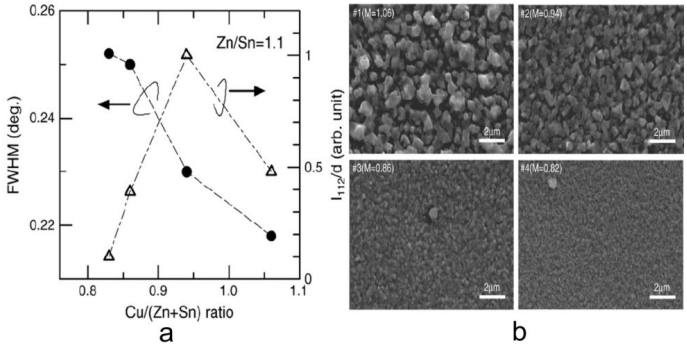

Figure 10. a) FWHM of the (112) diffraction peak and normalized (112) diffraction intensity of CZTS films (I_{112}/d) as a function of Cu/(Zn+Sn) ratio, (b) SEM surface images of CZTS films with different Cu/(Zn+Sn) ratios [79].

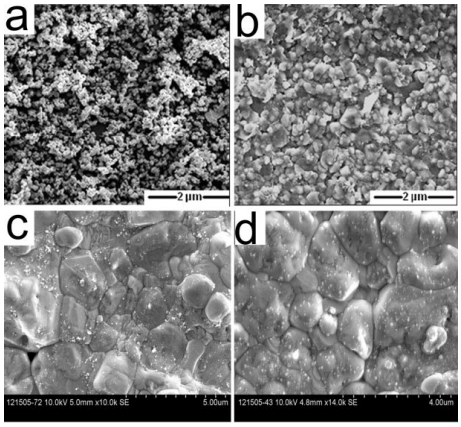

Figure 11. SEM surface images of CZTS thin films deposited on different substrates: (a) LAG, (b) SLG, (c) LAG, (d) SLG. [(a) and (b) were reported by Jampana et al. [83] (c) and (d) are results from our group].

All the reports showed that the conventional evaporation method is efficient for the development of CZTS TFSCs. However, non-uniformity caused by splash encountered in the evaporation of copper will significantly deteriorate the performance of CZTS module as does in the fabrication of CIGS module (Unpublished data). The fact that the commercial production capacity of CIGS solar modules by evaporation is far lower than that by sputtering is a perfect suggestion for CZTS solar industries [84]. More stable and controllable sputtering method is more readily applied to mass production of CZTS solar modules.

3.3.2. Sputtering

In 1988, Ito analyzed the electrical and optical properties of CZTS thin film which was deposited on slide glass substrate by atom beam sputtering [40]. The deposited CZTS thin film

http://dx.doi.org/10.5772/50702

was (112)-oriented and polycrystalline. The grain size increased when CZTS thin film was deposited at higher temperature because the mobility of sputtered particles was higher on the substrate surface (Fig. 12(a)). Its resistivity decreased from $4x10^4$ Ω•cm to 1.3 Ω•cm with the increase of deposition temperature (Fig. 12(b)). Hall-effect measurement estimated that CZTS thin film had mobility lower than 0.1 $cm^2 \bullet V^{-1} \bullet s^{-1}$ and the carrier concentration was higher than 5×10^{19} cm^{-3}. This CZTS thin film was considered optically desirable for the absorber layer of solar cell because the deposited CZTS thin film had an absorption coefficient larger than 1.2×10^4 cm^{-1} and a direct bandgap of 1.45 eV.

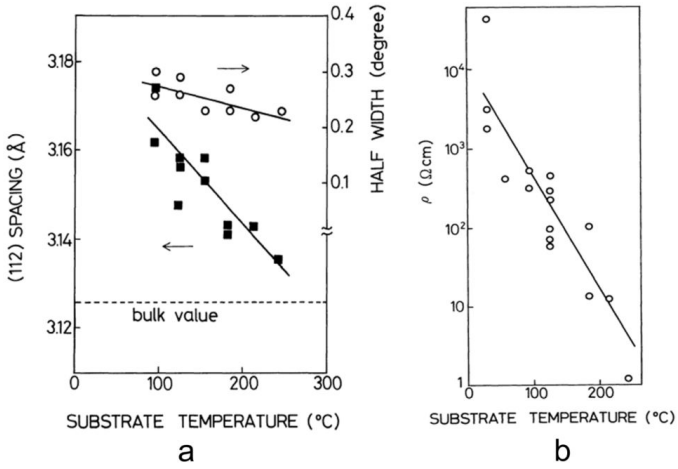

Figure 12. a) (112) plane spacing (■) and FWHM of the (112) peak (○) of CZTS, (b) the correlation between resistivity (ρ) of CZTS and substrate temperature [40].

In 2003, Seol et al. deposited CZTS films using RF-magnetron sputtering system and quaternary CZTS target (composed of finely mixed Cu_2S, ZnS and Sn_S2 at ratio of 2:1.5:1) followed by annealing in the atmosphere of Ar+S (g) [85]. The effects of sputtering power and annealing temperature on the properties of CZTS thin films were checked. It was found that the atomic ratio of the thin films obtained between 50 W and 100 W was appropriate. However, the Cu content of CZTS thin films was significantly decreased while the Sn content was rapidly increased with a power above 100 W. The authors suggested that the plasma density caused the abrupt changes of the Cu and Sn contents. CZTS thin films annealed at above 250 ℃ were (112)-oriented and other major diffraction peaks were assigned to (200), (220), and (312) planes. As annealing temperature increased, the intensity of the (112) peak was stronger.

In 2005, hybrid sputtering was employed by Tanaka et al. to prepare CZTS thin films [44]. The hybrid sputtering system was constructed in a deposition chamber with two effusion cells for Zn and S and two sputtering sources for Cu and Sn. CZTS thin films were fabricated by sequential deposition of Sn, Zn, and Cu followed by annealing in S vapor. The substrate temperature was varied between 300 ℃ and 500 ℃. The film thickness decreased with

increasing of substrate temperature. This was probably caused by the decrease of the sticking coefficient and/or by the increase of density due to crystallization at high temperature. CZTS thin films remained stoichiometric when the substrate temperature was elevated to up to 400 ℃. However, the composition of the thin films became Zn-poor at the substrate temperature above 450 ℃. At higher temperature, the vapor pressure of Zn is higher, leading to loss of Zn. It was proposed that Zn loss at higher substrate temperature could be prevented by using binary compound ZnS instead of Zn or by introducing S vapor during the deposition of Zn to form zinc sulfide on the surface of precursor.

CZTS precursor films are generally taken out of the deposition chamber and exposed to the atmosphere before sulfurization is performed to grow CZTS polycrystalline thin films. Moisture can be adsorbed on the surface of CZTS precursor films which is thereof oxidized during annealing at high temperature. Thus, in-line sulfurization should be capable of avoiding the problem. Jimbo et al. carried out this process with sputtered CZTS precursor films to curb the oxidization [57]. Targets of Cu, ZnS and SnS were simultaneously sputtered by RF sources. The finished precursor was automatically transferred to the annealing chamber without being exposed to atmosphere and annealed at 580 ℃ for 3 h in an atmosphere of N_2+H_2S (20%). Measurement data showed that annealed CZTS thin film had the thickness of 2.5 μm and bandgap of 1.45 eV. The film was copper-poor and slightly zinc-rich and sulfur-rich (Cu/Zn+Sn: 0.87, Zn/Sn: 1.15, S/metals: 1.17). The sample had an open circuit voltage of 662 mV, a short circuit current of 15.7 mA/cm^2, a fill factor of 55%, a conversion efficiency of 5.74%. The improved efficiency was attributed to the in-line annealing process and better CZTS morphology achieved.

	J_{SC} (mA/cm^2)	V_{OC} (mV)	*FF* (%)	R_S (Ω•cm^2)	R_{Sh} (Ω•cm^2)	η (%)
Before DI-water soaking	15.7	662	55	9.04	612	5.74
After DI-water soaking	17.9	610	62	4.25	370	6.77

Table 5. Comparison of *J-V* properties of CZTS solar cells treated with and without deionized-water soaking [57, 59].

In 2008, the champion efficiency for CZTS solar cell was achieved by Katagiri's group through preferential etching technique where the CZTS absorber layer on the Mo-coated SLG substrate was soaked in deionized water (DI-water) for 10 min before the CdS buffer layer was grown on the CZTS absorber layer using chemical bath deposition method [59]. The comparison of *J-V* properties was listed in Table 5. As we can see, DI-water soaking treatment CZTS absorber layer was very effective to improve the efficiency. The effect of the DI-water soaking on the oxygen distribution in CZTS thin film was studied by electron probe X-ray micro analysis (EPMA). Areas with higher concentration of oxygen are scattered in the CZTS layer before the soaking treatment (Fig. 13(a)). In contrast, the concentration of oxygen in the CZTS layer after the soaking treatment is lower than the measurement limit of the EPMA instrument (Fig. 13(b)). The authors suggested that oxygen removed was in the form of metal oxide because metal oxide nanoparticles are easy to dissolve in water. The removal of these metal oxide nanoparticles by DI-water is beneficial to improve the per-

http://dx.doi.org/10.5772/50702

formance of CZTS solar cell. On the one hand, more sunlight will be absorbed by CZTS, resulting in higher J_{SC} because free carriers will not be generated in the metal oxides as effectively as CZTS. On the other hand, the contact area between CdS buffer layer and CZTS absorber layer will be increased after the removal of metal oxide nanoparticles, leading to lower series resistance of CZTS PV device.

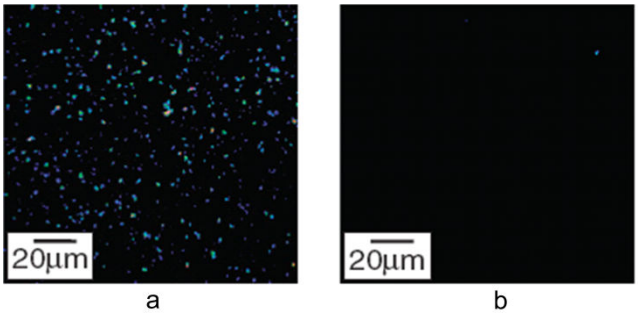

Figure 13. Distributions of oxygen in the CZTS layer before (a) and after (b) DI-water soaking for 4 h (bright areas are higher concentration areas of oxygen) [58].

As introduced above, the material properties of CZTS thin films and the performance of CZTS TFSCs are not only highly dependent on the deposition techniques but also dependent on how the sputtering target is made and what it is made of. The cooperation between PV device researchers and sputtering target vendors has to be intensified to make full use of their respective experiences and therefore to expedite the development of CZTS PV technology.

3.3.3. Pulsed laser deposition (PLD)

So far, laser has only successfully been applied to formation of interconnection paths between individual cells in series-connected solar modules such as a-Si, CdTe, and CIGS. In 2007, Moriya et al. deposited CZTS thin films on Mo-coated soda lime glass (SLG) substrate at room temperature using KrF excimer laser for ablating sintered CZTS pellets [68]. Annealing at 500 ℃ in N_2 was carried out for growing CZTS crystals. The CZTS TFSCs showed an open-circuit voltage of 546 mV, a short-circuit current of 6.78 mA/cm^2, a fill factor of 48% and a conversion efficiency of 1.74%.

In 2010, Pawar et al. investigated the effect of incident energy density of laser on the structural, morphological and optical properties of CZTS thin films using similar PLD method as reported previously [68, 86]. Laser incident energy density was changed from 1.0 J/cm^2 to 3.0 J/cm^2. XRD results indicated that the crystallinity of the as-deposited CZTS thin films was improved with the increase of laser incident density up to 2.5 J/cm^2. However, the film was slightly degraded when the laser energy density was further increased to 3.0 J/cm^2 due to the large plasma density and high kinetic energy induced by too intense laser. SEM surface images of the annealed CZTS thin films showed the average grain size increased, and these films be-

came relatively more uniform as the laser incident energy was increased from 1.0 to 2.5 J/cm^2. The bandgap decreased with the increase of laser incident energy up to 2.5 J/cm^2 as well.

The efficiency of CZTS solar cell fabricated by PLD was further improved to 3.14% in 2011 [69]. CZTS pellets were made from Cu_2S, ZnS, and SnS_2 mixed powders (molar ration of 1:1:1) which were synthesized by solid state reaction method. CZTS thin films were then deposited by PLD method in high vacuum using the CZTS pellets as source. These films were further annealed under N_2 (95%) + H_2S (5%) atmosphere at 400 ℃ for 1 h. The best CZTS solar cell reported in this work had a V_{OC} of 651 mV, an I_{SC} of 8.76 mA/cm^2, and a *FF* of 55%.

3.3.4. Non-vacuum processes

Cost-effectiveness is the core of the development of any new technology. Total abandonment of vacuum facilities in the manufacture of PV systems is the best way to further lower the cost of PV modules. Several non-vacuum methods have been successfully employed in the development of CZTS TFSCs.

3.3.4.1. Electrodeposition

The first CZTS solar cell deposited using electrodeposition was achieved by Scragg et al. [41]. In this method, copper chloride, tin chloride and zinc chloride were separately dissolved in a mixture solution containing NaOH and sorbitol. Metal layers were potentiostatically deposited at room temperature in the order Cu, Sn, Zn using a conventional 3-electrode electrochemical cell with a platinum counter electrode and Ag/AgCl reference electrode. The electroplated metallic films and sulfur powder were loaded into a graphite container, which was inserted into a furnace tube. CZTS thin films were then synthesized at 550 ℃ by the sulfurization of the electroplated metallic films. The fabricated solar cell demonstrated an efficiency of 0.8% with an open circuit voltage of 295 mV, a short circuit current density of 8.7 mA/cm^2, and a fill factor of 32%.

The crystallization and sulfurization processes of the elecrodeposited CZTS precursor films were investigated by Schurr et al. using angle-dispersive time-resolved XRD measurements [87]. Two different types of precursor films with copper-rich and copper-poor ratios in the as-deposited films were checked. It was found that the kesterite crystallization was completed by the solid state reaction of Cu_2SnS_3 and ZnS in both cases. However, in-situ XRD data showed reaction path for the formation of Cu_2SnS_3 depended on the metal ratios in the as-deposited films. The reaction schemes were derived from time-resolved XRD results and shown below. The reactions can be described below.

For copper-rich samples,

$$2Cu_3Sn + 7S \rightarrow 3Cu_2 - xS + 2SnS_2; \quad (4)$$

$$2CuZn + 3S \rightarrow Cu_{2-x}S + 2ZnS; \quad (5)$$

http://dx.doi.org/10.5772/50702

$$Cu_{2-x}S + SnS_2 \rightarrow Cu_2SnS_3; \quad (6)$$

$$Cu_2SnS_3 + ZnS \rightarrow Cu_2ZnSnS_4; \quad (7)$$

For copper-poor samples,

$$Cu_6Sn_5 + S \rightarrow SnS_2 + Cu_{2-x}S + Cu_3Sn; \quad (8)$$

$$2Cu_2S + SnS_2 + 2S \rightarrow Cu_4SnS_6; \quad (9)$$

$$Cu_4SnS_6 \rightarrow 2Cu_{2-x}S + SnS_2(melted) + 2S; \quad (10)$$

$$Cu_{2-x}S + SnS_2(melted) \rightarrow Cu_2SnS_3; \quad (11)$$

$$Cu_2SnS_3 + ZnS \rightarrow Cu_2ZnSnS_4; \quad (12)$$

These reactions also indicate how the sulfurization and crystallization are completed in CZTS precursor films deposited using vacuum-based technologies since these methods usually involve similar precursors.

In 2009, Ennaoui et al. achieved an efficiency of 3.4% using electrodeposited copper-poor CZTS thin film as absorber layer [61]. The formation of the binary sulfides and the thereof resulted liquid phase could contribute to the enhancement of kesterite crystal growth.

In 2012, electrodeposited CZTS solar cell with an efficiency of 7.3% was fabricated by Deligianni et al. using a three-step method [74]. Firstly, metal stacks of either Cu/Zn/Sn or Cu/Sn/Zn were electrodeposited. Secondly, low temperature annealing at 210–350 °C in N_2 was employed to produce homogeneous (Cu, Zn) and (Cu, Sn) alloys. Lastly, these well-mixed CuZn and CuSn alloys were annealed at 550 –590 °C in sulfur vapor for 5 to 15 min. A single highly crystalline CZTS phase was achieved. This is so far the record efficiency for electrodeposited CZTS solar devices.

3.3.4.2. Sol-gel method

CZTS precursor sol-gel was made by dissolving copper (II) acetate monohydrate, zinc (II) acetate dehydrate and tin (II) chloride dehydrate in mixture solution of 2-methoxyethanol (2-metho), deionized water and binder and then spin-coated on Mo-coated soda lime glass substrates followed by drying at 300 ℃ on a hot plate [67]. The coating and drying process were repeated several times. Lastly, the precursors were annealed at 500 ℃ in an atmosphere of N_2 +H_2S (5%). The CdS layer was grown on CZTS thin film by the chemical bath deposition (CBD) method. The CdS thickness was optimized by changing deposition time from 5 to 25 minutes. It was found that sample with CdS thin film deposited for 23 minutes showed the best conversion efficiency (J_{SC}=6.70 mA/cm^2, V_{OC}=554 mV, *FF*=43.4%, η=1.61%).

Tanaka et al. fabricated a CZTS solar cell with all semiconductor layers being coated by non-vacuum deposition techniques [66]. The ZnO:Al window layer and the CZTS absorber layer were deposited using sol-gel method. CdS buffer layer was coated by chemical bath deposition method. CZTS precursor thin films were coated using sol–gel solution of Cu, Zn, and Sn ions. Sulfurization was employed at 500 ℃ under a mixture atmosphere of H_2S and N_2 with H_2S concentration changing from 3% to 20%. CZTS thin film prepared with a H_2S concentration of 3% had grains with size of 1 μm. The best solar cell, which was obtained from a sample sulfurized at a H_2S concentration of 3%, demonstrated a conversion efficiency of 2.23%. This is so far the highest efficiency for sol-gel method deposited CZTS solar cells.

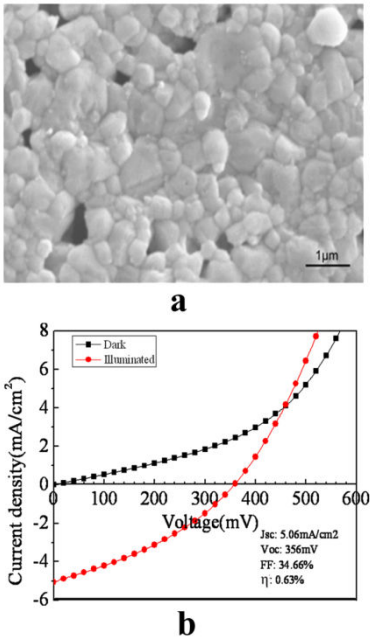

Figure 14. a) SEM surface image of CZTS thin film, (b) typical J-V curve of CZTS TFSC deposited by sol-gel method [27].

We have deposited CZTS thin films by employing sol-gel method [26]. The deposited CZTS thin film consisted of large densely packed grains with size of more than 400 nm (Fig. 14(a)) and had an optical bandgap of 1.51 eV. The compositional ratios could be optimized through modification of the composition of CZTS sol-gel precursor and annealing processes. An efficiency of 0.63% has been demonstrated (Fig. 14(b)). The relatively low efficiency resulted from the low V_{OC} and *FF* which was caused by the cracks and penetrating pores generated during the annealing process. With this ongoing project, we have already improved FF by 19% using ~ 450 nm thick CZTS film by controlling the deposition process, leading to significant improvement of morphology (Fig. 15). A multiple layer deposition process successfully blocked the penetrating pores.

http://dx.doi.org/10.5772/50702

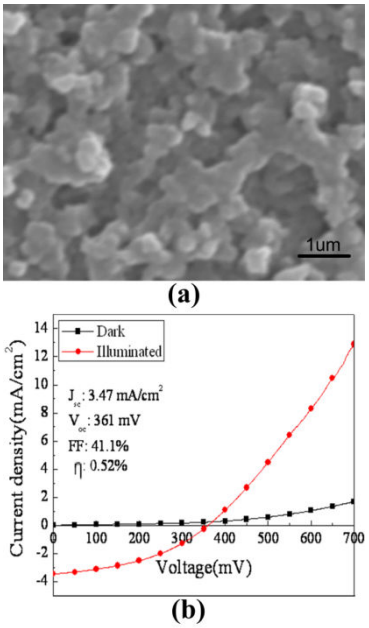

Figure 15. a) SEM surface image and (b) J-V property of CZTS TFSC with improved morphology.

3.3.4.3. Nanoparticle-based method

Hot-injection method is usually employed to synthesize CZTS nanoparticles [88, 89]. In a typical synthesis, copper salt, zinc salt, and tin salt are dissolved in oleylamine. The mixture solution is heated to 130 ℃ under inert atmosphere. The temperature is then raised to 225 ℃ where mixture solution of sulfur and oleylamine is injected. The mixture is then cooled to 80 ℃. Organic solvents such as toluene and isopropanol are added into the reaction mixture where CZTS nanoparticles are collected using centrifuge. Steinhagen et al. fabricated a CZTS PV device by dispersing CZTS nanoparticles in toluene (20 mg/mL) and spray coating the CZTS layer on CdS/ZnO-coated indium tin oxide (ITO) glass [71]. A typical CZTS solar cell showed an open-circuit voltage of 321 mV, a short-circuit current density of 1.95 mA/cm^2, a fill factor of 37%, and a conversion efficiency of 0.23%.

High quality CZTS nanocrystals with well controlled size, shape, and chemical composition have been successfully synthesized [90-93]. Nevertheless, to what extent these properties will affect CZTS TFSCs has rarely been addressed and needs to be further explored. Annealing procedure has to be applied to CZTS nanocrystals to grow polycrystalline CZTS thin films. Cracking and material loss encountered in other methods must be prevented to achieve CZTS polycrystalline thin film with high semiconductor quality. For more details, we recommend the recently published review paper by Lin et al. about nanoparticle-based method for CZTS TFSCs [94].

3.3.4.4. Screen-printing

Zhou et al. produced CZTS ink by dispersing CZTS microparticles in mixture solution of isopropanol and ethyl cellulose [72]. CZTS thin film with thickness of about 3 μm was screen printed on Mo-coated glass substrate and then was dried naturally. Organic materials were removed using a hot roll at 195 ℃. I-V measurement of a typical CZTS solar cell showed the feasibility of this method to be used to make CZTS solar cell (J_{SC}=4.76 mA/cm^2, V_{OC}=386 mV, *FF*=0.27, η=0.49%). The authors speculated that the comparatively low efficiency could attribute to internal deficiencies in the screen-printed CZTS solar cells, such as high contact resistance between CZTS paste and Mo conductive layer and small amount of residual oxide in the precipitate.

Screen-printing technology has been successfully applied on Si wafer-based PV technologies, which partly contributed to rapid decrease of the price of Si wafer-based PV modules. However, screen-printing process is widely employed to prepare the front and back metal contacts. The p-n junction formed using screen-printing method has yet to be proved to be successful due to non-uniformity generated in the screen-printed film and carbon-based solvents employed in the preparation of paste. Considering the high sensitivity of CZTS thin film to composition variation, it will be more difficult to achieve desirable CZTS absorber layer using screen-printing technology.

The demonstrated performance of CZTS TFSCs by these methods is lower than those by vacuum-based method. However, non-vacuum-based techniques such as nanoparticle-based method and sol-gel method are promising because of simplicity and versatility associated with these methods.

4. Prospects

The efficiency of CZTS solar cell has been significantly improved since 2000. Due to know-how gained from the research on CIGS solar module, an efficiency of 6.21% has been realized for CZTS solar module with an aperture area of 22.6 cm^2 [50]. Collaboration to market CZTS PV technology has been laid ground among semiconductor industry and photovoltaic industry giants [95, 96]. However, a number of technical issues must be addressed and corresponding solutions are provided before CZTS PV technology becomes marketable.

4.1. Defect engineering

4.1.1. Defect control

Defect states in quaternary compounds such as CIGS and CZTS thin films are very complicated. As introduced above, vacancies such as V_{Cu}, V_{Zn}, V_{Sn}, and V_S, antiesite defects such as Cu_{Zn}, Zn_{Cu}, Cu_{Sn}, Sn_{Cu}, Zn_{Sn}, and Sn_{Zn}, intrinsic defects such as Cu_i, Zn_i, and Sn_i are possible to form during deposition of CZTS thin film. The formation energy of acceptor defects was lower than that of donor defects, which makes p-type self-doping comparably easy in CZTS. The commonly observed p-type conductivity of CZTS thin films mainly arises from the Cu_{Zn} antisite defect. Successfully fabricated CZTS solar cells are usually Cu-poor and Zinc-rich.

http://dx.doi.org/10.5772/50702

On the one hand, the conductivity of CZTS thin film derived from intrinsic defects helps to minimize extrinsic defects which have a high density in highly phosphor-doped Si to form emitter which is usually called as dead region because most of photon-excited free carriers recombine at defect states. On the other hand, the electrical properties of CZTS thin film are extremely difficult to be precisely controlled. As far as composition concerned, the transition region from being highly efficient to being dead is very narrow as is CIGS thin film solar cell. Defect engineering such as Na incorporation and Sb doping have been successfully employed for CIGS thin film to extend the region and henceforth improve the efficiency. Similar experiments could benefit CZTS solar cell as well because CZTS has a lot in common with CIGS. Most researchers have been dedicating their efforts in developing novel deposition methods for CZTS thin film. The research focus will soon be turned to defect engineering once the newly developed deposition methods gain maturity.

4.1.2. Pure CZTS phase generation and secondary phase detection

The investigation on the phase equilibrium in the Cu_2S-ZnS-SnS_2 system showed that single-phase CZTS crystals can only be grown in a very narrow region (Fig. 16) [97]. To form pure CZTS phase is a challenge. Secondary phases such as ternary and quaternary compounds are much easier to form than CZTS. Therefore, it is quite challenging to deposit CZTS thin film without significant presence of secondary phases. Time-resolved XRD measurements clearly illustrated that the crystallization of kesterite CZTS was completed by the solid state reaction of Cu_2SnS_3 and ZnS whatever the precursor was [85]. The formation of binary and ternary secondary phases including Zn_xS, Cu_xS, Sn_xS, and Cu_xSnS_y are often observed during and after the growth of CZTS crystals.

Highly performed CZTS solar cells are slightly Zn-rich and Cu-poor. However, secondary phases such as ZnS and Cu_2SnS_3 are readily to be formed during thin-film growth in a Zn-rich regime. Inhomogeneity due to the presence of these secondary phases was assumed to contribute to the comparatively low efficiencies. Detection of secondary phases will guide how to improve the growth method for CZTS thin film. Nevertheless, it is commonly recognized that detecting secondary phases using only XRD in CZTS is not as easy as in CIGS because kesterite CZTS shares multiple peaks with cubic ZnS and Cu_2SnS_3 (Fig. 17). Raman spectroscopy is often combined with XRD results to characterize CZTS thin films [30, 32].

Hartman et al. developed a technique defined as extended X-ray absorption fine structure (EXAFS) which is sensitive to local chemical environment and able to determine the quantity of ZnS phase in CZTS films by detecting differences in the second-nearest neighbor shell of the Zn atoms [98]. The results so far are promising. Significant differences in EXAFS spectra with varying amounts of Zn and Cu in the CZTS films have been observed. Further work is required to quantify the amount of secondary ZnS phase in EXAFS spectra and to enable EXAFS technique to be confidently employed in characterizing CZTS thin film.

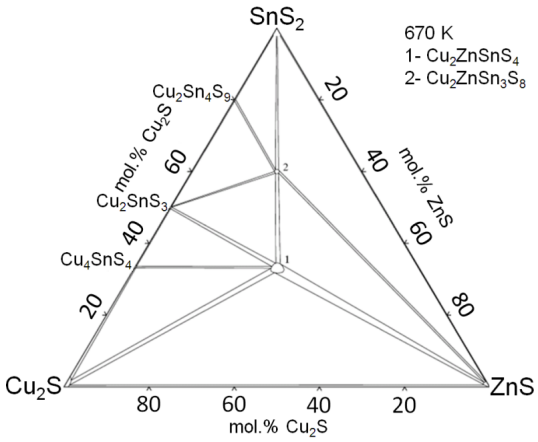

Figure 16. Phase diagram of SnS_2-Cu_2S-ZnS system [97].

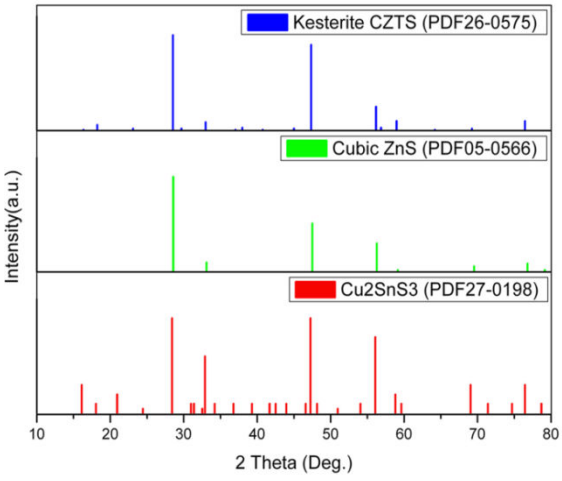

Figure 17. Comparison of XRD peaks of CZTS, ZnS, and Cu_2SnS_3.

4.2. Bandgap engineering

Bandgap tuning has been widely and successfully employed in fabrication of CIGS TFSCs. Techniques such as substitution of In by Ga and replacement of Se by S can precisely control the bandgap of CIGS thin film [99-102]. The performance of CIGS TFSCs was significantly improved not only because gradient bandgap was introduced into the absorber layer but also because the conduction band offset (CBO) between buffer layer and CIGS absorber layer was optimized through tuning the conduction band of CIGS thin film [103,105]. This pro-

http://dx.doi.org/10.5772/50702

vides CZTS TFSC researchers with another powerful technology to improve the efficiency of CZTS TFSC.

Theoretical calculation and experimental results demonstrated that the bandgap of CZTS nanocrystal could also be controlled through incorporation of Se [105]. Zhang et al. analyzed experimentally and theoretically the effects of Se incorporation on the bandgap of CZTS nanocrystal. It was found that band gap of CZTS nanocrystal demonstrated a parabolic nature. The bandgap firstly decreased with the increase of Se/(S + Se) ratio and then increased with the increase of Se/(S + Se) ratio when the ratio was higher than 0.55 (Fig 18). The variation range of optical band gap for CZTS nanocrystal is from 1.28 eV to 1.5 eV.

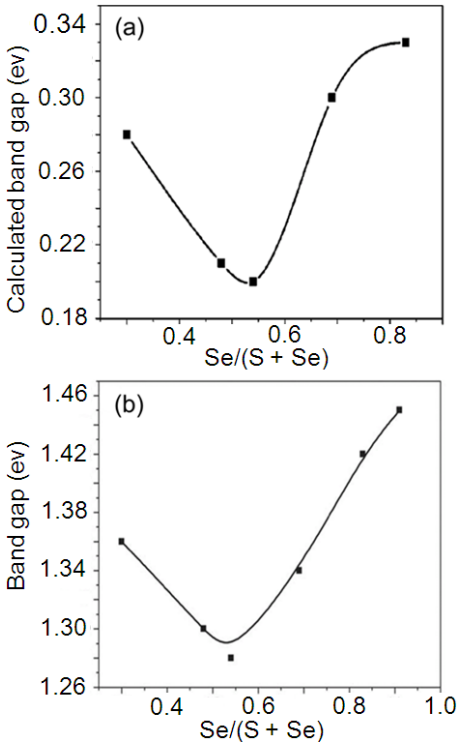

Figure 18. The dependence of bandgap of $Cu_2ZnSnS_{4x}Se_{4(1-x)}$ nanocrystals on the ratio of Se/(Se+S): (a) theoretical results, (b) experimental results [105].

The control of bandgap of CZTS nanocrystal was also realized by Agrawal et al. [106]. $GeCl_4$ was added into the reaction solution to partly replace tin (IV) acetylacetonate dichloride. TEM images and XRD data indicated that the $Cu_2ZnSn_{1-x}Ge_xS_4$ (CZTGS) nanocrystals varying in size from 5 to 30 nm were successfully produced. UV-Vis results for CZTGS nanocrystals indicated that the bandgap of CZTGS nanocrystals increased with the increase of Ge/(Sn +Ge) ratio (Fig. 19). CZTGS TFSCs with comparatively high efficiency have been fabricated

after selenization. The highest efficiency for CZTGS TFSCs was achieved from the cell with a Ge/(Sn+Ge) ratio of 6.8% (Table 6). This efficiency is slightly lower but comparable to that of CZTGS TFSC without Ge incorporation.

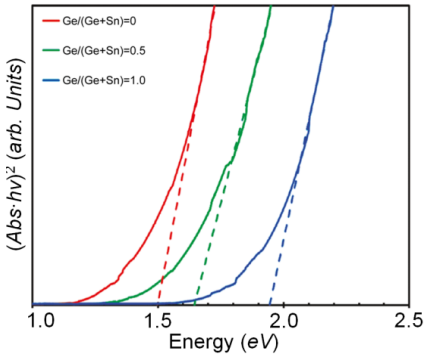

Figure 19. Absorbance of CZTGS nanocrystals with different ratio of Ge/(Ge+Sn) [106].

	Ge/(Ge+Sn)=0	Ge/(Ge+Sn)=0.7	Ge/(Ge+Sn)=1.0
J_{SC} (mA/cm^2)	31.2	21.5	4.7
V_{OC} (mV)	430	640	320
FF (%)	54	49	33.7
R_S (Ω)	4.9	9.1	30.5
R_{Sh} (Ω)	850	460	269
η (%)	7.2	6.8	0.51

Table 6. J-V properties of CZTGS TFSC with different ratio of Ge/(Ge+Sn) [106].

The widening effect of bandgap through Ge incorporation and the narrowing effect of bandgap through Se incorporation facilitate the design of high efficiency CZTS TFSC based on multi-junction (Fig. 20). Interfacial recombination caused by crystal mismatch will be minimized due to the high similarity of crystal structures among these materials.

4.3. Toxic element-free

Toxic chemicals are widely and heavily consumed in the manufacturing process of PV industry. The environmental damage could be minimized if the wastes were well treated because they are usually confined in a certain area. Nevertheless, toxic elements contained in PV modules have potential to polluting the earth because a large amount of PV modules are required to be installed in the desert and on residential roofs to power households. Lives

could be lost due to the emission of toxins during fire. Toxic element-free PV technologies will be more preferred when solar electricity is selected to be main power source.

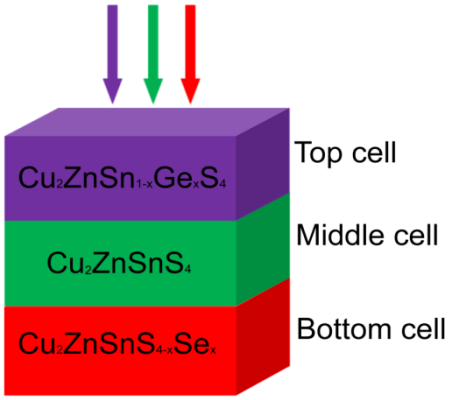

Figure 20. Proposed multi-junction CZTS solar cell.

4.3.1. Selenium-free

Selenium compounds such as hydrogen selenide are extremely toxic while selenium itself is not highly toxic. Selenization and sulfurization are often employed to CZTS precursors to grow high quality CZTS thin films. The efficiency of CZTS solar cell is lower than that of CZTSSe solar cell which is incorporated with selenization (Table 7) [36]. The authors concluded that the comparatively low efficiency associated with CZTS and CZTSSe solar cells were caused by the extremely low lifetime because a typical lifetime of a high quality CIGS device is beyond 50 ns. The differences of J_{SC} and V_{OC} were mainly due to the difference of optical bandgap. The difference between the efficiencies of CZTS and CZTSSe PV devices was probably from the difference of bandgap which attributed to unfavourable band alignments with the CdS emitter layer, leading to higher series resistance.

	Thin film		Solar cell				
	Bandgap (eV)	Lifetime (ns)	J_{SC} (mA/cm^2)	V_{OC} (mV)	*FF* (%)	η (%)	R_S (Ω•cm^2)
CZTS	1.45	0.78	21.0	614	55.3	7.13	7.4
CZTSSe	1.17	0.50	29.5	422	60.0	7.51	1.5

Table 7. Comparison of properties of CZTS and CZTSSe TFSCs [36].

For solution-based CZTS solar cells, selenium incorporation plays an even greater role in improving the efficiency of CZTS solar cell. Firstly, Se has higher reactivity than S. Metals in

CZTS precursors will more readily react with Se to produce metal selenides and consequently to grow CZTSSe thin films. Phase separation in sulfurized CZTS thin film is more common than that in selenized CZTS thin film. Secondly, CZTS thin film is usually deposited at so high a temperature that cracks are highly possible to be generated due to volume contraction caused by evaporation of metal sulfides and excess sulphur [107]. Displacement of S with Se during selenization can prevent crack forming because the aomic radius of selenium is larger than that of sulfur

However, knowledge achieved from fabrication of CIGS solar cell can shed light on how to make selenium-free CZTS solar cell with high efficiency. It was reported that CIGS solar cell showed higher efficiency when deposited under heat-cracked selenium vapor because cracked selenium vapor is more reactive than selenium vapor without cracking treatment which mainly consists of Se_8 [108]. Cracking treatment for sulfur vapor has been first employed to fabricate CZTS solar cell by IBM [36]. Treatment details were not available. It would be a feasible method to improve the quality of CZTS thin film in that sulfur vapor is mainly composed of S_8 which has lower reactivity than S as does Se_8 than Se. Moreover, CIGS solar cell with high efficiency has been successfully fabricated by ISET who synthesized copper oxide, indium oxide, and gallium oxide nanoparticles as precursors [109]. Similar technology can be developed to deposit CZTS thin film. Synthesis of nanoparticles of copper oxide, zinc oxide, and tin oxide has been widely reported in literatures. Volume contraction will be minimized if sulfurization is employed to CZTS precursors containing these metal oxide nanoparticles because the atomic radius of S is larger than that of O as is Se larger than S. It was found that zinc oxide was easily turned into zinc sulfide after being annealed in a mixture atmosphere of hydrogen sulfide, hydrogen, and nitrogen [110]. Similar methods have yet proved to be possible to produce copper sulfide and tin sulfide. It would be a novel technology to fabricate selenium-free CZTS solar cell with high efficiency once the methods are available.

4.3.2. Cadmium-free

CdS thin film is commonly incorporated in CZTS PV device as buffer layer to form p-n junction with p-type CZTS absorber layer. However, the environmental risk brought by the implementation of CdS is nontrivial when CZTS PV technology is widely employed, not to mention the marketing problem caused by legal regulations of Cd in electrical or electronic equipment in different countries [111, 112]. Free carriers excited by photons with energy ranging from 2.3 eV to 3.6 eV are lost in CdS thin film. The elimination or replacement of CdS thin film has potential of increasing photocurrent generated in this energy region, and therefore improving the cell efficiency.

So far, Cd-free CZTS solar cells have been reported by just a few groups [50, 70, 113]. The buffer layers employed and *J-V* properties are summarized in Table 8. Solar Frontier has successfully fabricated a Cd-free CZTS sub-module [50]. The Zn-based buffer layer was deposited by chemical bath deposition on CZTS thin film coated by sulfurization of an evaporated stacking precursor. It was interesting that the efficiency of the Zn-based buffer sub-module was higher than that of the Cd-based buffer sub-module even if the Zn-based buffer

cell fabricated with same batch of CZTS had lower efficiency than the Cd-based buffer cell. The authors attributed the enhancement of efficiency to the higher transparency and improvement of shunt resistance, resulting in higher external quantum efficiency, *EQE*, higher J_{SC} and higher V_{OC}.

Buffer layer	J_{SC} (mA/cm^2)	V_{OC} (mV)	*FF* (%)	η (%)	Aperture area (cm^2)	Year	Reference
ZnS	8	410	35.5	1.16	unavailable	2011	[69]
ZnS(O,H)	15.77	618	59.8	5.82	0.54	2011	[97]
Cd-free sub-module	10.30	631	30.7	2.01	21.8	2011	[49]

Table 8. *J-V* properties of Cd-free CZTS PV devices.

Excitingly, our tests demonstrated that the efficiency of Cd-free CIGS solar cell had been significantly improved to be over that of Cd-based CIGS solar cell through modifying the composition of CIGS absorber (unpublished data). Similar results (Table 9) have also been observed for CZTS solar cell [50]. The efficiency decreased with the decrease of the ration of Zn to Sn for Cd-based CZTS solar cell. However, the contrary was true for Cd-free CZTS solar cell. The champion efficiency of 5.82% for Cd-free CZTS solar cell was obtained at a Zn/Sn ratio of 1.02. Efforts have to be focused on not only the successful deposition of Cd-free buffer layer but also the optimization of the whole PV device [114].

Zn/Sn	Power conversion efficiency (%)	
	Cd-based	Cd-free
0.99	4.24	4.33
1.24	5.09	3.69
1.50	6.08	3.00

Table 9. Efficiencies of Cd-based and Cd-free CZTS PV devices depend on the ratio of Zn to Sn [50]

4.4. Nanostructured CZTS solar cell

Nanostructured PV devices have gained tremendous interest since the advent of dye-sensitized solar cell [115-117]. Organic semiconductors have absorption coefficients as high as 10^5 cm^{-1} but exciton diffusion length as low as tens of nanometers. Nanostructure provides excitons with high possibility to be dissociated before they recombine [118]. Furthermore, efficient light trapping associated with nanostructure reduces the amount of deposited absorber materials [119]. Also, nanostructures are compatible with printing PV technology based on nanoparticles, leading to reduction of processing costs and energy pay-back time of solar cells.

Nanostructured CZTS solar cell has not been reported although ZnO nanorod coated on ITO has been successfully applied to CIGS solar cells [120]. The efficiency was improved for

nanostructured CIGS solar cell compared to planar one. However, the efficiencies are much lower than those of conventional CIGS solar cells fabricated on Mo-coated glass. It was assumed that organic materials contained in the CIGS precursors sprayed on ZnO nanorods could not be totally eliminated, leading to degradation of CIGS thin film. Moreover, the annealing temperature cannot be as high as that employed in the fabrication of conventional CIGS solar cells because ITO thin film will be damaged under S or Se vapor, leading to poorer crystal qualities of CIGS thin film.

Therefore, we propose a nanostructured CZTS PV device based on Mo nanorods and sol-gel derived CZTS thin film (Fig. 21). Mo thin film and Mo nanorods are sequentially deposited on glass [Fig. 21(a)]. CZTS sol-gel precursor is then spin-coated on Mo nanorods [Fig. 21(b)]. Annealing at high temperature is employed to grow CZTS polycrystalline thin film. Lastly, CdS, i-ZnO, and TCO are sequentially coated on CZTS polycrystalline thin film [Fig. 21(c) and Fig. 21(d)]. The advantages of nanostructure and conventional CZTS will be integrated in a single PV device.

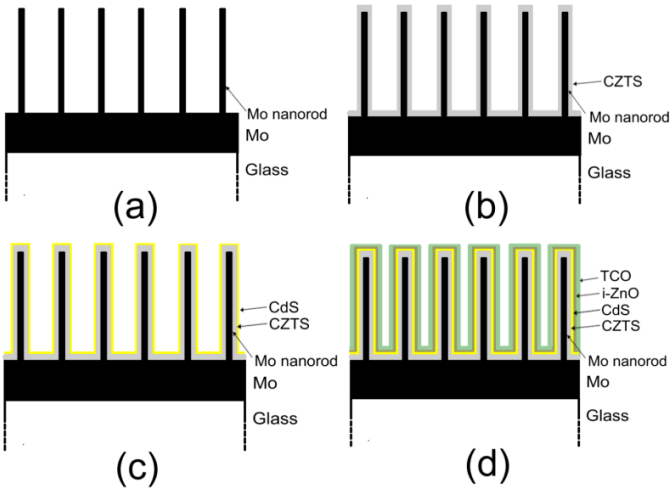

Figure 21. Proposed nanostructured CZTS PV device.

5. Remarks and conclusions

The tremendous progresses recently achieved on CZTS have demonstrated the potential of fabricating high-performance and cost-effective PV devices with low environmental pollution. Both vacuum-based and non-vacuum-based methods have been successfully explored to fabricate CZTS solar cells. Among vacuum-based methods, evaporation and sputtering are appropriate deposition techniques in terms of efficiencies. Non-vacuum-based techni-

http://dx.doi.org/10.5772/50702

ques including nanoparticle-based and sol-gel methods are also promising because of simplicity. To further improve the performance of CZTS solar cells, intensive efforts should be committed to the development of the approaches for forming pure CZTS phase and the detection techniques of secondary phases formed during the deposition of the CZTS thin film. Also, research efforts need to be focused on cadmium-free and selenium-free CZTS PV technologies. Further improvement can be expected in that know-how of CIGS PV technology and related nanotechnology is readily transferred to the research of CZTS PV technology due to great similarity between these two materials. A maturated CZTS PV technology is expected for the TFSC family in a near future.

Acknowledgements

We acknowledge the financial support from the NASA through Contract NNX09AU83A.

Author details

Minlin Jiang and Xingzhong Yan

*Address all correspondence to: xingzhong.yan@sdstate.edu

Department of Electrical Engineering and Computer Science, South Dakota State University, SD, 57007, USA

References

[1] Husser, P., Watt, G., & Kaizuka, I. *Proceedings 17 17th International PVSEC 2007*, 1110-1113.

[2] Honda, J. *Proceedings 17 17th International PVSEC 2007*, 114.

[3] Wortmann, D. *Proceedings 17th International PVSEC 2007*, 120.

[4] European commissions. http://ec.europa.eu/dgs/jrc/index.cfm.

[5] Solarbuzz. http://www.solarbuzz.com/news/NewsNACO1205.htm.

[6] Von, Roedern. B., Zweibel, K., & Ullal, H. S. *Proceedings 31 31st PVSC 2005*, 183-188.

[7] Komoto, K., Uchida, H., Ito, M., Kurokawa, K., & Inaba, A. *Proceedings 23rd European Photovoltaic Solar Energy Conference and Exhibition 2008*, 3833-3835.

[8] Aydil, E.S. http://www1.umn.edu/iree/e3/archive/archive_2010/E3_Aydil.pdf.

[9] Green, M. A. *Prog. Photo volt.Res. Appl.*, 17-347.

[10] Wadia, C., Alivisatos, A. P., & Kammen, D. *Environ. Sci. Technol. 2009*, 43, 2072-2077.

[11] Nische, R., Sargent, D. F., & Wild, P. J. *Cryst. Growth 1967*, 1, 52-53.

[12] Schäfer, W., & Nitsche, R. *Mat. Res. Bull. 1974*, 9, 645-654.

[13] Lu, X., Zhuang, Z., Peng, Q., & Li, Y. *Chem. Comm.*, 47-3141.

[14] Paier, J., Asahi, R., Nagoya, A., & Kresse, G. *Phys. Rev. B. 2009*, 115-126.

[15] Chen, S., Gong, X. G., Walsh, A., & Wei, S. (2009). *Appl. Phys.Lett*, 041-903.

[16] Wangperawong, A., King, J. S., Herron, S. M., Tran, B. P., Pangan-Okimoto, K., & Bent, S. F. *Thin Solid Films 2011*, 519, 2488-2492.

[17] Zhang, X., Shi, X., Ye, W., Ma, C., & Wang, C. *Appl. Phys. A 2009*, 94-381.

[18] Pawar, S. M., Pawar, B. S., Moholkar, A. V., Choi, D. S., Yun, J. H., Moon, J. H., Kolekar, S. S., & Kim, J. H. *Electrochim Acta.*, 55-4057.

[19] Zhou, Y., Zhou, W., Du, Y., Li, M., Wu, S., & Mater, Lett. (20116). 65-1535.

[20] Araki, H., Kubo, Y., Jimbo, K., Maw, W. S., Katagiri, H., Yamazaki, M., Oishi, K., & Takeuchi, A. *Phys. Status. Solidi 2009*, 6, 1266-1268.

[21] Araki, H., Mikaduki, A., Kubo, Y., Sato, T., Jimbo, K., Maw, W. S., Katagiri, H., Yamazaki, M., Oishi, K., & Takeuchi, A. *Thin Solid Films 2008*, 517, 1457-1460.

[22] Araki, H., Kubo, Y., Mikaduki, A., Jimbo, K., Maw, W. S., & Katagiri, H. *Sol. Energy. Mater Sol. Cells 2009*, 93, 996-999.

[23] Katagiri, H., Ishigaki, N., Ishida, T., Saito, K., & Jpn, J. *Appl. Phys. 2001*, 40, 500-504.

[24] Cao, M., & Shen, Y. J. *Cryst. Growth 2011.*, 318, 1117-1120.

[25] Katagiri, H., Saitoh, K., Washio, T., Shinohara, H., Kurumadani, T., & Miyajima, S. *Sol. Energy. Mater Sol. Cells 2001.*, 65, 141-148.

[26] Jiang, M., Dhakal, R., Li, Y., Thapaliya, P., & Yan, X. *Proceedings 37 37th IEEE PVSC2011 (Seattle, USA).*

[27] Jiang, M., Li, Y., Dhakal, R., Thapaliya, P., Mastro, M., Caldwell, J. D., Kub, F., & Yan, X. J. *Photon Energy 2011.*, 1, 019501.

[28] Wang, X., Sun, Z., Shao, C., Boye, D. M., & Zhao, J. *Nanotechnology 2011*, 22, 245605.

[29] Fontané, X., Calvo-Barrio, L., Izquierdo-Roca, V., Saucedo, E., Pérez-Rodriguez, A., Morante, J. R., Berg, D. M., Dale, P. J., & Siebentritt, S. *Appl. Phys. Lett. 2011.*, 98, 181905.

[30] Yoo, H., & Kim, J. *Thin Solid Films*, 518-6567.

[31] Wang, K., Shin, B., Reuter, K. B., Todorov, T., & Mitzi, D. B. *Appl. Phys. Lett. 2011.*, 98, 051912.

[32] Chalapathy, R. B. V., Lee, C., & Ahn, B. T. *Proceedings 37th IEEE PVSC 2011 (Seattle, USA)*.

[33] Unold, T., Kretzschmar, S., Just, J., Zander, O., Schubert, B., Marsen, B., & Schock, H. *Proceedings 37th IEEE PVSC 2011 (Seattle, USA)*.

[34] Miyamoto, Y., Tanaka, K., Oonuki, M., Moritake, N., Uchiki, H., & Jpn, J. *Appl. Phys.*, 47, 596-597.

[35] Leitão, J. P., Santos, N. M., Fernandes, P. A., Salomé, P. M. P., da, Cunha. A. F., González, J. C., & Matinaga, F. M. *Thin Solid Films 2011.*, 519, 7390-7393.

[36] Shin, B., Wang, K., Gunawan, O., Reuter, K. B., Chey, S. J., Bojarczuk, N. A., Todorov, T., Mitzi, D. B., & Guha, S. *Proceedings 37th IEEE PVSC2011 (Seattle, USA)*.

[37] Chen, S., Yang, J., Gong, X., Walsh, A., & Wei, S. *Phys. Rev. B. 2010*, 245204.

[38] Moriya, K., Tanaka, K., & Uchiki, H. *Jpn. J. Appl. Phys. 2008*, 47, 602-604.

[39] Jun, Z., & Xi, S. *Sci. China. Ser-TechE. Sci. 2009.*, 52, 269-272.

[40] Ito, K., & Nakazawa, T. *Jpn. J. Appl. Phys. 1988.*, 27, 2094-2097.

[41] Scragg, J. J., Dale, P. J., Peter, L. M., Zoppi, G., & Forbes, I. Phys. Stat. Sol. B. 2008 , 245, 1772-1778.

[42] Fernandes, P. A., Salomé, P. M. P., da Cunha, A. F., & Schubert, B. Thin Solid Films 2011. , 519, 7382-7385.

[43] Liu, F., Zhang, K., Lai, Y., Li, J., Zhang, Z., & Liu, Y. *Electrochem-StateSolid.Lett. 2011*, H379-H381.

[44] Tanaka, T., Nagatomo, T., Kawasaki, D., Nishio, M., Guo, Q., Wakahara, A., Yoshida, A., & Ogawa, H. J. *Phys. Chem. Solids 2005.*, 66, 1978-1981.

[45] Rajeshmon, V. G., Kartha, C. S., Vijayakumar, K. P., Sanjeeviraja, C., Abe, T., & Kashiwaba, Y. *Sol. Energy. 2011.*, 85, 249-255.

[46] Liu, F., Li, Y., Zhang, K., Wang, , Yan, C., Lai, Y., Zhang, Z., Li, J., & Liu, Y. *Sol. Energy. Mater Sol. Cells 2010*, 94, 2431-2434.

[47] Chan, C. P., Lam, H., & Surya, C. *Sol., Energy. Mater Sol. Cells 2010.*, 94, 207-211.

[48] Wagner, S., & Bridenbaugh, P. M. J. *Cryst. Growth. 1977.*, 39, 151-159.

[49] Katagiri, H., Sasaguchi, N., Hando, S., Hoshino, S., Ohashi, J., & Yokota, T. *Sol. Energy. Mater. Sol. Cells 1997.*, 49, 407-414.

[50] Hiroi, H., Sakai, N., & Sugimoto, H. *Proceedings 37th IEEE PVSC 2011 (Seattle, USA)*.

[51] Kobayashi, T., Jimbo, K., Tsuchida, K., Shinoda, S., Oyanagi, T., & Katagiri, H. *Jpn. J. Appl. Phys. 2005.*, 44, 783-787.

[52] Schubert, B., Marsen, B., Cinque, S., Unold, T., Klenk, R., Schorr, S., & Schock, H. *Prog. Photovolt. Res. Appl. 2011.*, 19, 93-96.

[53] Weber, A., Krauth, H., Perlt, S., Schubert, B., Kötschau, I., Schorr, S., & Schock, H. W. *Thin Solid Films 2009.*, 2524-2526.

[54] Katagiri, H., Jimbo, K., Moriya, K., & Tsuchida, K. *Proceedings 3rd World Conference on Photovoltaic Energy Conversion 2003.*, 3, 2874-2879.

[55] Redinger, A., Berg, D. M., Dale, P. J., & Siebentritt, S. J. *Am. Chem. Soc. 2011.*, 133, 3320-3323.

[56] Wang, K., Gunawan, O., Todorov, T., Shin, B., Chey, S. J., Bojarczuk, N. A., Mitzi, D., & Guha, S. *Appl. Phys. Lett. 2010.*, 143508.

[57] Jimbo, K., Kimura, R., Kamimura, T., Yamada, S., Maw, W. S., Araki, H., Oishi, K., & Katagiri, H. *Thin Solid Films 2007.*, 515, 5997-5999.

[58] Katagiri, H., & Jimbo, K. *Proceedings 37th IEEE PVSC 2011 (Seattle, USA).*

[59] Katagiri, H., Jimbo, K., Yamada, S., Kamimura, T., Maw, W. S., Fukano, T., Ito, T., & Motohiro, T. *Appl. Phys. Express 2008.*, 041201.

[60] Scragg, J. J., Berg, D. M., & Dale, P. J. J. *Electroanal Chem. 2010.*, 646, 52-59.

[61] Ennaoui, A., Lux-Steiner, M., Weber, A., Abou-Ras, D., Kötschau, I., Schock, H., , W., Schurr, R., Hölzing, A., Jost, S., Hock, R., Vo, T., Schulze, J., & Kirbs, A. *Thin Solid Films*, 517, 2511-2514.

[62] Araki, H., Kubo, Y., Jimbo, K., Maw, W. S., Katagiri, H., Yamazaki, M., Oishi, K., & Takeuchi, A. *Phys. Status. Solidi 2009*, 96, 1266-1268.

[63] Araki, H., Kubo, Y., Mikaduki, A., Jimbo, K., Maw, W. S., Katagiri, H., Yamazaki, M., Oishi, K., & Takeuchi, A. *Sol. Energy. Mater Sol. Cells 2009.*, 996-999.

[64] Tanaka, K., Fukui, Y., Moritake, N., & Uchiki, H. *Sol. Energy. Mater. Sol. Cells 2011*, 95, 838-842.

[65] Tanaka, K., Oonuki, M., Moritake, N., & Uchiki, H. *Sol. Energy. Mater Sol. Cells 2009*, 93, 583-587.

[66] Maeda, K., Tanaka, K., Fukui, Y., & Uchiki, H. *Sol. Energy. Mater Sol. Cells 2011.*, 95, 2855-2860.

[67] Moritake, N., Fukui, Y., Oonuki, M., Tanaka, K., & Uchiki, H. *Phys. Status. Solidi 2009*, 1233-1236.

[68] Moriya, K., Tanaka, K., & Uchiki, H. *Jpn. J. Appl. Phys. 2007*, 46, 5780-5781.

[69] Moholkar, A. V., Shinde, S. S., Babar, A. R., Sim, K., Lee, H., Rajpure, K. Y., Patil, P. S., Bhosale, C. H., & Kim, J. H. J. *Alloys Compd. 2011.*, 509, 7439-7446.

[70] Prabhakar, T., & Nagaraju, J. *Proceedings 37th IEEE PVSC 2011 (Seattle, USA).*

[71] Steinhagen, C., Panthani, M. G., Akhavan, V., Goodfellow, B., Koo, B., & Korgel, B. A. J. *Am. Chem. 2009.*, 12554-12555.

[72] Zhou, Z., Wang, Y., Xu, D., & Zhang, Y. *Sol. Energy. Mater Sol. Cells 2010.*, 94, 2042-2045.

[73] Shin, B., Gunawan, O., Zhu, Y., Bojarczuk, N. A., Chey, S. J., Guha, S., & Prog, Photovolt. *Res.Appl. 2011.*, DOI:10.1002/pip.1174.

[74] Ahmed, S., Reuter, K. B., Gunawan, O., Guo, L., Romankiw, L. T., & Deligianni, H. *Adv. Energy. Mater 2012.*, 2, 253-259.

[75] Repins, I., Contreras, M. A., Egaas, B., De Hart, C., Scharf, J., Perkins, C. L., To, B., & Noufi, R. *Prog. Photovolt. Res. Appl. 2008.*, 16, 235-239.

[76] Barkhouse, D. A. R., Gunawan, O., Gokmen, T., Todorov, T. K., & Mitzi, D. B. *Prog. Photovolt. Res. Appl. 2012.*, 20, 6-11.

[77] Guo, Q., Ford, G. M., Yang, W., Walker, B. C., Stach, E. A., Hillhouse, H. W., & Agrawal, R. J. *Am. Chem. Soc. 2010.*, 13, 17384-17386.

[78] Han, S., Hasoon, , S., F., Al-Thani, H. A., Hermann, A. M., & Levi, D. H. J. *Phys. Chem. Solids 2005.*, 66, 1895-1898.

[79] Tanaka, T., Yoshida, A., Saiki, D., Saito, K., Guo, Q., Nishio, M., & Yamaguchi, T. *Thin Solid Films 2010.*, S29-S33.

[80] Caballero, R., Kaufmann, C. A., Eisenbarth, T., Cancela, M., Hesse, R., Unold, T., Eicke, A., Klenk, R., & Schock, H. W. *Thin Solid Films 2009.*, 517, 2187-2190.

[81] Rudmann, D., Bilger, G., Kaelin, M., Haug, F. J., Zogg, H., & Tiwari, A. N. *Thin Solid Films 2001.*, 431-432, 37-40.

[82] Ye, S., Tan, X., Jiang, M., Fan, B., Tang, K., & Zhuang, S. *Appl. Opt. 2010.*, 49, 1662-1665.

[83] Prabhakar, T., & Jampana, N. *Sol. Energy. Mater. Sol. Cells. 2011.*, 95, 1001-1004.

[84] Waldau, A. J. *Sol. Energy. Mater. Sol. Cells 2011.*, 95, 1509-1517.

[85] Seol, J., Lee, S., Lee, J., Nam, H., & Kim, K. *Sol. Energy. Mater Sol. Cells 2003.*, 75, 155-162.

[86] Pawar, S. M., Moholkar, A. V., Kim, I. K., Shin, S. W., Moon, J. H., Rhee, J. I., & Kim, J. H. Curr. Appl. Phys. 2010. , 10, 565-569.

[87] Schurr, R., Hölzing, A., Jost, S., Hock, R., Vo, T., Schulze, J., Kirbs, A., Ennaoui, A., LuxSteiner, M., Weber, A., Kötschau, I., & Schock, H.W. Thin Solid Films 2009. , 517, 2465-2468.

[88] Riha, S. C., Parkinson, B. A., & Prieto, A. L. J. *Am. Chem. Soc. 2009.*, 12054-12055.

[89] Guo, Q., Hillhouse, H. W., & Agrawal, R. J. *Am. Chem. Soc. 2009.*, 131, 11672-11673.

[90] Kameyama, T., Osaki, K. T., Okazaki, Shibayama. T., Kudo, A., Kuwabatade, S., & Torimoto, T. J. *Mater Chem. 2010.*, 20, 5319-5324.

[91] Zhou, Y., Zhou, W., Li, M., Du, Y., & Wu, S. J. *Phys. Chem. C. 2011.*, 115, 19632-19639.

[92] Ching, J. Y., Gillorin, A., Zaberca, O., Balocchi, A., & Marie, X. *Chem. Commun. 2011.*, 47, 5229-5231.

[93] Shi, L., Pei, C., Xu, Y., & Li, Q. J. *Am. Chem. Soc. 2011.*, 133, 10328-10331.

[94] Wang, J., Xin, X., & Lin, Z. Nanoscale, 2011. , 3, 3040.

[95] PV magazine. http://www.pv-magazine.com/news/details/beitrag/solar-frontier-and-ibm-to-develop-czts-cell-100001390/.

[96] Business insider. http://www.businessinsider.com/delsolar-and-ibm-to-jointly-develop-czts-solar-cell-technology-20109.

[97] Oleksyuk, I. D., Dudchar, I. V., & Piskach, L. V. J. *Alloys Compd. 2004.*, 368, 135-143.

[98] Hartman, K., Newman, B. K., Johnson, J. L., Du, H., Fernandes, P. A., Chawla, V., Bolin, T., Clemens, B. M., da, Cunha. A. F., Teeter, G., Scarpulla, M. A., & Buonassisi, T. *Proceedings 37th IEEE PVSC 2011 (Seattle, USA).*

[99] Lundberg, O., Edoff, M., & Stolt, L. Thin Solid Films 2005. , 480-481, 520-525.

[100] Sakurai, K., Scheer, R., Nakamura, S., Kimura, Y., Baba, T., Kaufmann, C. A., Neisser, A., Ishizuka, S., Yamada, A., Matsubara, K., Iwata, K., Fons, P., Nakanishi, H., & Niki, S. *Sol. Energy. Mater Sol. Cells 2006.*, 90, 3377-3384.

[101] Jung, S., Ahn, S., Yun, J., Gwak, J., Kim, D., & Yoon, K. *Current Appl. Phys. 2010*, 10, 990-996.

[102] Li, W., Sun, Y., Liu, W., & Zhou, L. *Sol. Energy. 2006*, 80, 191-195.

[103] Nakada, T., Hongo, M., & Hayashi, E. Thin Solid Films 2003. , 431-432, 242-248.

[104] Minemoto, T., Hashimoto, Y., Kolahi, W., Satoh, T., Negami, T., Takakura, H., & Hamakawa, Y. *Sol. Energy. Mater Sol. Cells 2003.*, 75, 121-126.

[105] Wei, H., Ye, Z., Li, M., Su, Y., Yang, Z., & Zhang, Y. *Cryst. Eng. Comm. 2011.*, 13, 2222.

[106] Ford, G. M., Guo, Q., Agrawal, R., & Hillhouse, H. W. *Chem. Mater. 2011.*, 23, 2626-2629.

[107] Todorov, T., Mitzi, D. B., & Eur, J. *Inorg. Chem. 2010.*, 17, 17-28.

[108] Kawamura, M., Fujita, T., Yamada, A., & Konagai, M. J. *Cryst. Growth. 2009.*, 311, 753-756.

[109] International Solar Electric Technology. http://isetinc.com/technology-overview.php.

[110] Zhang, R., Wang, B., Wan, D., & Wei, L. *Opt. Mater. 2004.*, 27, 423-419.

http://dx.doi.org/10.5772/50702

[111] Hynes, K. M., & Newham, J. *Proceedings 16th European Photovoltaic Solar Energy Conference 2000*, 2297.

[112] Directive 2002/96/EC. *27 the European parliament and of the council of 27 January 2003 on waste electrical and electronic equipment (WEEE), Official Journal of the European Union (2003) L37/24.*

[113] Sakai, N., Hiroi, H., & Sugimoto, H. *Proceedings 37th IEEE PVSC 2011 (Seattle, USA).*

[114] Jiang, M., Tang, K., & Yan, X. J. *Photon Energy 2012 in progress.*

[115] Yang, H., Song, Q., Lu, Z., Guo, C., Gong, C., Hu, W., & Li, C. Energy Environ. Sci. 2000. , 3, 1580-1586.

[116] Wang, L. *Energy Environ. Sci. 2009.*, 2, 944-955.

[117] Muduli, S., Game, O., Dhas, V., Yengantiwar, A., & Ogale, S. B. *Energy Environ. Sci. 2011.*, 4, 2835-2839.

[118] Li, Y., Yan, M., Jiang, M., Dhakal, R., Thapaliya, P. S., & Yan, X. J. *Photon Energy 2011.*, 1, 011115.

[119] Kuang, Y., van der Werf, K.H.M., Houweling, Z. S., & Schropp, R. E. I. Appl. Phys. Lett. 2011. , 113111.

[120] Krunks, M., Katerski, A., Dedova, T., Acik, I. O., & Mere, A. Sol. Energy. Mater Sol. Cells 2008. , 92, 1016-1019.